sustainability

MDPI

Article

Analysis of COVID-19 Lockdown Effects on Urban Air Quality: A Case Study of Monterrey, Mexico

Benedetto Schiavo [1,*], Ofelia Morton-Bermea [1], Thania Elizabeth Arredondo-Palacios [2], Diana Meza-Figueroa [3], Agustin Robles-Morua [4], Rocío García-Martínez [2], Daisy Valera-Fernández [1], Claudio Inguaggiato [5] and Belem Gonzalez-Grijalva [3]

1 Instituto de Geofísica, Universidad Nacional Autónoma de México, Mexico City 04510, Mexico
2 Instituto de Ciencias de la Atmósfera y Cambio Climático, Universidad Nacional Autónoma de México, Mexico City 04510, Mexico
3 Departamento de Geología, Universidad de Sonora, Hermosillo 83000, Mexico
4 Departamento de Ciencias del Agua y del Medio Ambiente, Instituto Tecnológico de Sonora, Ciudad Obregón 85000, Mexico
5 Departamento de Geología, Centro de Investigación Científica y de Educación Superior de Ensenada, Baja California (CICESE), Ensenada 22860, Mexico
* Correspondence: benedetto@igeofisica.unam.mx

Abstract: The COVID-19 pandemic has caused several millions of deaths and forced the world population to a new normality. This study aims to analyze the air quality variation of several gaseous pollutants (CO, NO_2, SO_2, O_3, PM_{10}, and $PM_{2.5}$) during the pre-lockdown, lockdown, and unlock period in the city of Monterrey using ground-based measurements. In this research, we proposed to use a control period of previous years to identify parameter variation due to local climate. The results showed a drastic decrease in measured contaminants during the lockdown period as follows: SO_2 (−41.9%) > PM_{10} (−30.5%) > $PM_{2.5}$ (−25.6%) > NO_2 (−14.9%) > CO (−9.8%) compared to the control period (2017–2019). The O_3 was the only air pollutant that showed an opposite trend, increasing during lockdown (+15%) and unlock (+2.2%), whereas CO (−16.6%) and NO_2 (−30.6%) were further decreased. Moreover, using OMI/AURA satellite data, we detected a NO_2 tropospheric column reduction by −1.9% during lockdown concerning the same period in the control interval. Moreover, we found a significant improvement in the Air Quality Index (AQI) due to the lockdown. Our findings indicate an association between air pollutants and economic activity and can be used in future strategies to improve urban air quality.

Keywords: SARS-CoV-2; air quality; environmental pollution; lockdown; nitrogen dioxide; particulate matter; monterrey

Citation: Schiavo, B.; Morton-Bermea, O.; Arredondo-Palacios, T.E.; Meza-Figueroa, D.; Robles-Morua, A.; García-Martínez, R.; Valera-Fernández, D.; Inguaggiato, C.; Gonzalez-Grijalva, B. Analysis of COVID-19 Lockdown Effects on Urban Air Quality: A Case Study of Monterrey, Mexico. *Sustainability* **2023**, *15*, 642. https://doi.org/10.3390/su15010642

Academic Editor: Elena Cristina Rada

Received: 20 November 2022
Revised: 24 December 2022
Accepted: 28 December 2022
Published: 30 December 2022

1. Introduction

Air pollution has become a global concern, mainly in developing countries (e.g., Mexico) and industrialized areas. According to the World Health Organization (WHO) [1], every year, millions of people suffer premature death caused by air pollution [2,3]. Atmospheric particulate matter (PM) is one of the most harmful pollutants deteriorating urban air quality and public health [4]. Airborne PM is characterized by different sizes and chemical compositions, as well as a mixture of a solid and liquid phase in suspended particles [5]. Several acute and chronic problems are related to PM exposure, including allergic symptoms [6] and lung disease [7]. In Mexico, due to its rapid expansion, industrialization, and economic growth, air pollution is one of the most relevant environmental and social concerns [8]. Romero-Lankao et al. [9] studied different megacities and found similar pollution conditions and associated health risks regardless of the area and socioeconomic status. Specific actions focused on improving air quality have been implemented over the years [10,11], such as vehicle emissions and maintenance controls, the use of catalytic converters, the substitution of fuel oil in industry and power plants with natural gas, and a "no driving day" program. Despite implementing the environmental policy plans in Mexico City, Morton-Bermea et al. [12] reported a rising trend of PM_{10} (i.e., particulate matter with aerodynamic particles less than 10 μm) from 2004 to 2014; therefore, more effective actions need to be taken into consideration [13,14]. While the COVID-19 pandemic caused a reduction in mobility, it represents a unique opportunity to understand the effectiveness of these environmental policies.

The novel coronavirus COVID-19 disease caused by SARS-CoV-2 was reported for the first time in Wuhan, Hubei province of China, at the end of December 2019 [15]. Its rapid expansion around the world forced the WHO to declare the outbreak of a global pandemic on 11 March 2020 [16]. Many governments of different countries, following the WHO statement about COVID-19 global health concern, started with the coronavirus containment strategy by declaring significant shutdown/lockdown periods. The restriction included reducing non-essential services and industrial activities, tourism, mass congregation, working travel, and mobility flow to mitigate the COVID-19 infection rate. Lockdown periods have globally affected the production sectors causing severe socioeconomic complications [17,18]. On 13 July 2022, the global number of confirmed coronavirus number cases was 568,045,618, including 539,261,494 recovered and 6,388,488 deaths reported from 250 countries worldwide [19]. The development of the pandemic in Mexico is described as follows: at the end of January 2020, the Mexican government proposed a national Preparation and Response plan intending to prepare for the imminent arrival of the pandemic [20]. In Mexico, the first confirmed COVID-19 cases were reported in Mexico City and in the northern state of Sinaloa on 28 February. A few days later, many more cases were confirmed in various states of Mexico [21]. The first death of a patient diagnosed with COVID-19 was acknowledged on 18 March 2020. By 30 March 2020, a total of 1094 cases and 28 deaths were registered in the country. Due to COVID-19 disease, the General Health Council declared a sanitary emergency with the suspension of all non-essential activities starting from 1 April 2020. Furthermore, the Mexican Secretary of Health launches the social distance healthy program to prevent coronavirus infections. The government announced a "new normality time" by mid-May 2020 and a reopening of all activities by 1 June 2020 [22].

While the COVID-19 pandemic forced the entire world to change their everyday lifestyle, a drastic decrease in pollution levels has been observed due to coronavirus control actions and a mobility reduction [23]. In addition, the different confinement policies implemented in countries around the world allow the understanding of the effect of human activities on air quality. In Mexico, such policies are restricted to megacities such as Mexico City. Despite the unique opportunity that the lockdown provided to understand the effects of mobility reduction, limited studies have been conducted in Mexico for air quality during the lockdown period [24]. Kutralam-Muniasamy et al. [25] described the air quality of Mexico City with a focus on $PM_{2.5}$, PM_{10}, nitrogen dioxide (NO_2), sulfur dioxide (SO_2), carbon monoxide (CO), and ozone (O_3). Compared to the control period (2015–2019), Mexico City reported an estimated reduction between 16–36% of $PM_{2.5}$, PM_{10}, NO_2, SO_2, and CO). On the contrary, O_3 concentration registered an increase in 14%.

It is relevant to assess to what extent these variations are unique to a megacity. To answer this, we chose the city of Monterrey, which has particular climatic characteristics since it is located in a semi-desert area. In this paper, we analyzed the variations in air quality using ground-based data and satellite measurements in the Monterrey Metropolitan Area (MMA), the second-largest urban center and the economic engine of Mexico. The pollutant variation during the lockdown period in metropolises located in the desert area is relatively few studied. MMA is a megacity located in a desert area where the variety of contaminants can have a component that depends on anthropogenic and natural emissions (desert contribution). Furthermore, MMA is affected by the Mexican monsoon, which brings intense winds and heavy rains, which can locally alter the concentration of contaminants in the atmosphere. The main objective of this study is to investigate the impact of imposed lockdown on MMA air quality using criteria pollutants including CO, NO_2, SO_2, O_3,

$PM_{2.5}$, and PM_{10}, retrieved from 10 air quality monitoring stations situated around the city. We seek to identify the pollution sources and help municipal governments implement environmental policy programs to minimize human health risks. Furthermore, data were compared to the same period in the previous 3 years (control period) to understand the potential effects and relative emissions change during the lockdown in 2020. Finally, the obtained results are compared to those found in Mexico City.

2. Methodology

2.1. Site Overview

The city of Monterrey is located in Nuevo Leon state (25°40′17″ N 100°18′31″ W), in the northeast of Mexico, with an average altitude of 550 m.a.s.l. (Figure 1). Due to the orographic formations, the city is surrounded by mountains, the Sierra Madre Oriental at the south (2400 m.a.s.l. of altitude) and the Sierra de la Silla at the west (between 1200 and 1800 m.a.s.l.). According to the 2020 statistical census [26], the population was approximately 1,142,953.

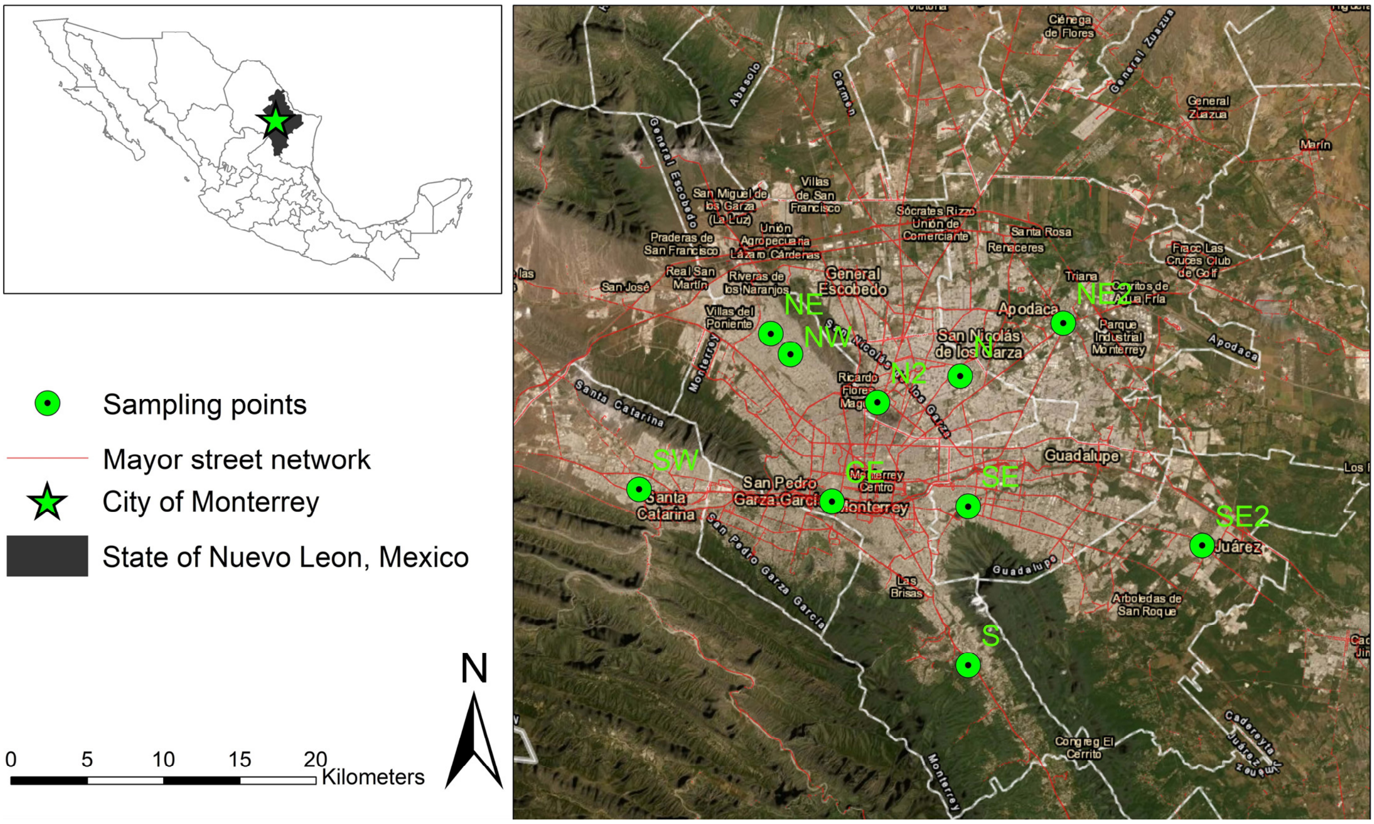

Figure 1. Location map of the Monterrey Metropolitan Area (MMA), Mexico. Green circles indicate the site of the air quality monitoring stations.

On the other hand, 5,341,174 inhabitants were registered in the MMA, converting it to the second most populated city in Mexico. The study area is characterized by urbanization, high traffic density, and an important industrial district. The industrial activities are situated in specific areas of the city, principally in the east and south. Instead, the residential and commercial areas are condensed close to the city center with a high traffic index. In Monterrey, following the Köppen climate classification [27], the climate is semiarid (warm and dry), classified as BSh. The seasons are well-defined, primarily during summer, which features a meteorological phenomenon called “Canicula,” characterized by no rainfall, heavy drought, and elevated temperature. The average annual temperature ranges between 16 and 28 °C with an average daily temperature of ~22 °C. The warmest months are July and August, with average and absolute recorded temperatures of about 29 and 35 °C, respectively. The average annual precipitation is approximate 600 mm, mainly in late summer and fall. The rainiest month is September, with an average precipitation of 150 mm and a relative humidity of 70%.

2.2. Air Quality Data Collection

The integrated environmental monitoring system (SIMA, Sistema Integral de Monitoreo Ambiental) has been operating since 1992, determining the levels of environmental contamination and air quality in the MMA. Currently, the network has 14 fixed monitoring stations for gas pollutants and selected meteorological parameters. Raw data provided by SIMA stations are automatically transferred to a central database, stored for quality control (i.e., statistical treatment, control, and validation), presented through monthly reports, and available upon explicit request. The location of the network monitoring stations (Figure 1) and the air quality status is available on the SIMA website (http://aire.nl.gob.mx/ (accessed on 10 October 2022)).

In this study, the hourly average concentrations of six air pollutants criteria (CO, NO_2, SO_2, O_3, PM_{10}, and $PM_{2.5}$) at ten monitoring stations (Table 1) in the city of Monterrey were obtained from SIMA. The concentrations of PM_{10}, $PM_{2.5}$, and CO were measured at all stations. Instead, O_3 and NO_2 were measured at seven stations, and SO_2 was measured at eight stations. Data reported by SIMA monitoring stations were not continuous, and in some cases, no records were registered in a certain period for a given gas pollutant. For this reason, during the whole study period, not all stations were considered. In the case of CO and O_3, the daily maximum 8-h moving average has been considered, following the Mexican legislation [28,29] and WHO guideline value [30]. The Federal Government of Mexico establishes permissible air concentration limits for each criterion pollutant to protect public health [31–35]. Mexican Official Regulations (NOM) publish the standard air quality applicable at a national scale. Specific reference values of air quality standard limits are described in Table 2. Furthermore, the days exceeding the WHO limits for each pollutant are also calculated [36]. According to WHO guideline limits of CO, NO_2, SO_2, O_3, PM_{10}, and $PM_{2.5}$ for 24-h (8-h for O_3) are 3.5 ppm, 13 ppb, 15 ppb, 50 ppb (daily maximum), 45 µg m^{-3}, and 15 µg m^{-3}, respectively. Instead, the annual limits for NO_2, PM_{10}, and $PM_{2.5}$ are 5 ppb, 15 µg m^{-3}, and 5 µg m^{-3}, respectively [37].

Table 1. Summary of selected air quality stations situated in the Monterrey Metropolitan Area (MMA), used in the present study.

Stations	Code	Latitude	Longitude	Air Pollutants	Site Description
Escobedo	N	25.745	100.255	PM_{10}–$PM_{2.5}$–CO	Urban area with a low impact of industrial activities.
San Bernabé	NW	25.757	100.366	PM_{10}–$PM_{2.5}$–O_3–CO–SO_2	Urban area with medium flow of vehicular traffic and low impact of industrial activities.
Obispado	CE	25.670	100.338	PM_{10}–$PM_{2.5}$–NO_2–O_3–CO–SO_2	Urban area with vehicular traffic in the neighborhood and without industrial impact.
Universidad	N2	25.729	100.309	PM_{10}–$PM_{2.5}$–NO_2–O_3–CO–SO_2	High impact of vehicular and industrial traffic, urban density north of the station.
La Pastora	SE	25.668	100.249	PM_{10}–$PM_{2.5}$–O_3–CO–SO_2	Commercial activities and vehicular flow, urban density west of the station.

Table 1. *Cont.*

Stations	Code	Latitude	Longitude	Air Pollutants	Site Description
San Nicolás	NE	25.769	100.379	PM_{10}–$PM_{2.5}$–NO_2–O_3–CO–SO_2	Urban area, with low vehicular activity, industrial activity to the north and east of the station.
Apodaca	NE2	25.777	100.188	PM_{10}–$PM_{2.5}$–NO_2–CO	Commercial and industrial activities, with a high impact of vehicular traffic and neighborhood areas.
Pueblo Serena	S	25.574	100.248	PM_{10}–$PM_{2.5}$–O_3–CO–SO_2	Urban area with high vehicular traffic in the neighborhood and without industrial impact.
Juárez	SE2	25.646	100.096	PM_{10}–$PM_{2.5}$–NO_2–CO–SO_2	Commercial activities and vehicular flow, urban density in the around, to east is ubicated a refinery oil.
Santa Catarina	SW	25.676	100.464	PM_{10}–$PM_{2.5}$–NO_2–O_3–CO–SO_2	Industrial activities to west and north, urban areas and commercial activities in the around, vehicular traffic in the neighborhood.

Table 2. Mexican air quality norm, standard limits, and instrumental techniques for each pollutant criterion.

Pollutant	Mexican Norm	Limit Description	Instrumental Technique
CO	NOM-021-SSA1-2021	Hourly mean: 26 ppm 8-h moving average: 9 ppm	Infrared photometry, Model 48C Operational range: 1–1000 ppm Detection limit: <0.5 ppm Flow rate: 0.5 L min^{-1}
NO_2	NOM-023-SSA1-2021	Hourly mean: 106 ppb Annual mean: 21 ppb	Gas phase chemiluminescence, Model 42C Operational range: 0.05–20 ppm Detection limit: <0.40 ppb Flow rate: 0.6 L min^{-1}
SO_2	NOM-022-SSA1-2019	24 h mean: 40 ppb Annual mean: 75 ppb	Ultraviolet fluorescence, Model 43C Operational range: 0.05–100 ppm Detection limit: <1.0 ppb Flow rate: 0.5 L min^{-1}
O_3	NOM-020-SSA1-2021	Hourly mean: 90 ppb 8-h moving average: 65 ppb	Ultraviolet spectrophotometry, Model 49C Operational range: 0.05–200 ppm Detection limit: <1 ppb Flow rate: 1 to 3 L min^{-1}
PM_{10}	NOM-025-SSA1-2014	24 h mean: 50 μg m^{-3} Annual mean: 35 μg m^{-3}	β-radiation attenuation, Model BEM 1020 Operational range: 0–1000 μg m^{-3} Detection limit: <1.0 μg m^{-3} Flow rate: 16.70 L min^{-1}
$PM_{2.5}$	NOM-025-SSA1-2014	24 h mean: 30 μg m^{-3} Annual mean: 10 μg m^{-3}	β-radiation attenuation, Model BEM 1020 Operational range: 0–1000 μg m^{-3} Detection limit: <1.0 μg m^{-3} Flow rate: 16.70 L min^{-1}

In addition, we determined the Air Quality Index (AQI) to evaluate the health benefit related to the lockdown period. The AQI is a helpful tool that allows accessible communication with the population, warning about the quality of the air and the potential health effects in a specific urban area. The AQI of the air pollutants was classified into six different levels and calculated as the following equation [38]:

$$I = \frac{I_{high} - I_{low}}{C_{high} - C_{low}} \times (C - C_{low}) + I_{low} \tag{1}$$

where I is the AQI for a specific air pollutant, C is the concentration of the air pollutant, C_{high} and C_{low} are the breakpoint (BP) of upper ($\geq C$) and lower (($\leq C$) concentrations, and I_{high} and I_{low} are the BP index corresponding to C_{high} and C_{low}. AQI values range from 0 to 500: 0–50 indicating *good* air quality, 51–100 indicating that air quality is *moderate*, and 101–150 indicating *unhealthy for sensitive groups* (i.e., children, older adults, and people with co-morbidity). Moreover, values in the range of 151–200, 201–300, and 301–500 indicate *unhealthy*, *very unhealthy*, and *hazardous* air quality conditions, respectively [39,40].

2.3. Instrumentations

Table 2 shows the details about detection limits, operational range, and other technical specifications of the instruments. The measurement instruments used in the SIMA air quality monitoring stations follow standard methods and principles by The United States–Environmental Protection Agency (U.S. EPA). The primary devices used in this work are the Infrared photometry for CO, gas phase chemiluminescence for NO_2, ultraviolet fluorescence, and spectrophotometry for SO_2 and O_3, respectively, and β-radiation attenuation for PM_{10} and $PM_{2.5}$.

The analyzer model 48C measures CO concentrations using infrared light in a wavelength of 4.6 microns. The sample enters the instrument and passes through an optical setting until it reaches a gaseous filter composed of CO and nitrogen (N). The artificial infrared radiation passes through the filter and makes contact with the sample. The radiation is absorbed by the CO at a specific wavelength and then is identified by infrared detectors, which convert it into concentration value. Calibration of the 48C model requires a CO standard reference material (SRM) by the National Institute of Standards and Technology (NIST) and a zero-air generator with a CO concentration of less than 0.01 ppm.

The gas phase chemiluminescence model 42C is based on the chemical principle by which the nitric oxide (NO) and the O_3 react, as expressed with the following formula:

$$NO + O_3 \rightarrow NO_2 + O_2 + h\nu \tag{2}$$

Once the reaction is complete, a characteristic luminescence is produced whose intensity is linearly proportional to the NO concentration. The sample flows through a particulate filter and a solenoid valve. The solenoid valve directs the sample to the reaction chamber with a mode to measure NO and NO_x. The difference between the concentrations is used to calculate the NO_2 concentration. Furthermore, with the possibility of injecting dry air into the device, the ozonator generates the necessary concentration for the chemiluminescence reaction. Ozone reacts with NO from the ambient air sample to produce electronically excited NO_2 molecules. A photomultiplier tube placed in a thermoelectric cooler detects the luminescence of NO_2 and converts the signal to concentration. The analyzer requires a zero-air source and no contamination by NO, NO_2, and O_3 for the calibration and dilution procedure. The molecules of SO_2 absorb fluorescence ultraviolet (UV) light, get excited at a specific wavelength in a range of 190–230 nm, and after passing to a lower state of energy, emit UV light in a different wavelength, as described by the following formula:

$$SO_2 + h\nu_1 \rightarrow SO_2^{*} \rightarrow SO_2 + h\nu_2 \tag{3}$$

The sample enters the analyzer model 43C by flowing through a kicker that blocks hydrocarbons. Afterward, the sample enters the fluorescence chamber, where SO_2 molecules are excited by pulses of UV light. Finally, excited SO_2 molecules are passed by the band filter and return to their normal state emitting UV light proportional to the SO_2 concentration. An initial calibration by model 43C is needed to obtain the quality assurance required for the measuring network. A zero-air source with a concentration of $SO_2 < 0.0005$ ppm is required to achieve an adequate calibration.

The spectrophotometry analyzer model 49C used UV light at a defined wavelength of 254 nm, which is absorbed by O_3 molecules. The level of UV absorption is related to O_3 concentration as described by the Beer-Lambert law [41]:

$$\frac{I}{I_0} = e^{-KLC} \tag{4}$$

where I is the intensity of UV light in the sample, I_0 is the intensity of UV light in the reference material, K is the absorption coefficient (308 cm^{-1}), L is the length of the cell (38 cm), and C is the O_3 concentration (ppm). Once the sample is obtained, it separates into two streams inside the analyzer. One flow passes through an O_3 scrubber and is used as a reference, and the other is directed toward the solenoid valve. Both gases are analyzed by detectors A and B, which measure the light's intensity and convert it into the O_3 concentration. No contaminated zero-air generator is necessary for device calibration.

The concentrations of PM_{10} and $PM_{2.5}$ were measured using an automatic analyzer BAM-1020 based on the physical principle of beta ray attenuation. The beta rays are generated by a 14C (carbon-14) source, which emits a constant flux of high-energy electrons. During an hour, the vacuum pump collects a controlled amount of ambient dust. The dust, once placed between the beta rays' source and the detector, causes the attenuation of the beta ray's signal. The attenuation is used to determine the PM mass and estimate the volumetric PM concentration in the air. The calibration of BAM-1020 consists of an accurate flow rate control with a traceable flow audit standard.

The analyzed gas pollutants follow rigorous quality assurance and control (QA/QC), and calibration protocols established by USEPA. The instruments used in the monitoring network are synchronized and have a temporal resolution of 1-h. The anomalous values were filtered based on lognormal distribution. The measurement accuracy of all instruments was approximately 95%.

2.4. Study Period

Although Mexico detected its first coronavirus case in late February, the restricted lockdown period (characterized by the shutdown of non-essential activities) was implemented on 1 April 2020. Furthermore, to compare pollutant concentrations during the lockdown to historical data, the same period of data from 2017 to 2019 was considered to compare pollutant concentrations during the lockdown to historical data. Therefore, the study period before lockdown, lockdown, and unlock phases during 2020 is described as follows:

1. **Pre-Lockdown (PL):** from 1 January to 31 March 2020 (normal economic and business activities, continuous monitoring of the coronavirus infection, and occasional reports on the local and global spread of COVID-19).
2. **Lockdown (L)**: from 1 April to 30 May 2020, significant public policy changes were implemented (substantial restrictions were imposed, such as stopping non-essential activities (mobility, industry, and school, among others).
3. **Unlock (UL):** from 1 June to 31 July 2020 (restart normal economic activities with some restrictions: people with co-morbidities continue with remote working, and schools have a hybrid condition, presential and online classes. Therefore, social distancing and using a face mask are strongly recommended).

The relative change (RC) between years and lockdown phases of air pollutants was calculated using the following equations:

$$Difference\ between\ years\ (\%) = \frac{GC\ (2020) - AGC\ (2017 - 2019)}{AGC\ (2017 - 2019)} \times 100 \tag{5}$$

$$Difference\ between\ lockdown\ phases\ (\%) = \frac{GC\ (L) - GC\ (BL)}{GC\ (BL)} \times 100 \tag{6}$$

where *GC* (2020) is the gas concentration of pollutants during 2020, *AGC* (2017–2019) is the average gas concentration during 2017–2019, *GC* (*L*) is the gas concentration during the lockdown period in 2020, and *GC* (*BL*) is the gas concentration before lockdown period in 2020. This study calculates percentage (%) change for *L* concerning the PL phase. Spatial and temporal variations were considered in the estimation of the RC.

2.5. Mobility Data

For this work, mobility data were downloaded and processed to evaluate Monterrey´s mobility trends within the studied periods. Daily mobility data were collected from "COVID-19 Mobility Reports" prepared by Google in February 2020 [42] for public health and used to analyze changes in mobility and how they affected the air quality in urban areas. Google reports mobility data (availability on https://www.google.com/covid19/mobility/ (accessed on 15 October 2022)) of the lockdown, before and after the lockdown period, from different countries worldwide, including Mexico. Google mobility data are divided into six different categories [42]: (i) retail and recreation, (ii) park, (iii) pharmacy, (iv) transit station, (v) workplace, and (vi) residential. The mobility percent changes in each category are estimated considering a baseline, the median value from the five weeks from 3 January to 6 February 2020. The mobility data were retrieved using the geolocation present in the most common mobile device.

2.6. Satellite Data Collection

Satellite-based remote sensing is widely exploited to simultaneously monitor different trace gas in the atmosphere simultaneously on a global scale [43]. Recently, during the COVID-19 pandemic, the retrieval of contaminated gases from satellite data has been widely used for creating concentration maps, comparison with control periods, and validation with ground-based measurement [44,45]. Since October 2004, Ozone Monitoring Instrument (OMI) has been located onboard the NASA AURA satellite. In the normal operation mode, the OMI ground pixel size varies from 13 km $\times$ 24 km with a sun-synchronous polar orbit. AURA/OMI monitoring satellite data (https://daac.gsfc.nasa.gov/ (accessed on 15 November 2022)) has been used to assess air quality changes of tropospheric contaminating gases during studied periods over Monterrey city. In order to retrieve the NO_2 (molecules/cm^2) concentrations, satellite data with the following characteristics were used: level 3 (global $OMNO_2$ v003) tropospheric column, 30% cloud screened, with a resolution of 0.25 $\times$ 0.25 degree.

2.7. Statistical Analysis

Basic statistics calculation was used to describe daily average concentrations, variation, and relative changes (%) during, before, and after each studied pollutant´s lockdown phase in 2020. Additionally, a statistical comparison with the control period (2017–2019) was reported for the same study period and stations. The time series plot of air contaminants and people mobility was performed using Python programming language, version 3.7.10 [46]. A Pearson correlation (r) was conducted between variables in the study period. Furthermore, a statistically significant difference was tested using a *t*-test (two-tailed) at a 95% confidence level ($\rho < 0.05$). Pollutants that reported r values lower than 0.5 are considered weakly correlated.

3. Results and Discussion

3.1. Mobility and Transport Variation during the Study Period

Mobility is a fundamental part of life and allows social interaction and human cognitive development [47]. Globally, the recent pandemic caused a considerable reduction in population mobility, as reported by several of the published literature [48–50]. A drastic reduction in mobility trends and social gatherings was registered in the MMA during the outbreak of COVID-19 (Figure 2). The mobility restriction intends to reduce the transmission rate of acute respiratory syndrome due to coronavirus diffusion. Nouvellet et al. [51]

reported a correlation between mobility reduction and decreasing COVID-19 cases. The analyzed categories, described in Section 2.5, show a similar variation during L, except residential, which increased by about 20.2%. The same trends are reported in different parts of the world [50,52]. This difference can be explained by considering a more significant amount of time spent in own residence. The restrictions strongly impacted the transit stations, followed by recreation, parks, and workplaces, with an average decrease compared to baseline of −59.5%, −54.1%, −49.4%, and −42%, respectively. Due to the need to find necessities and medicines, the mobility trends to groceries and pharmacies were higher than other categories, with a decrease in −16.7%. The workplace mobility, even recording a sharp decrease, shows a substantial variability during the study period, mainly due to the continuity of some essential activities during L, such as public health (e.g., hospital), emergency services (e.g., police and fireman), food and agriculture, energy production, and government operations. Excluding residential, mobility decreased by about −44.3%.

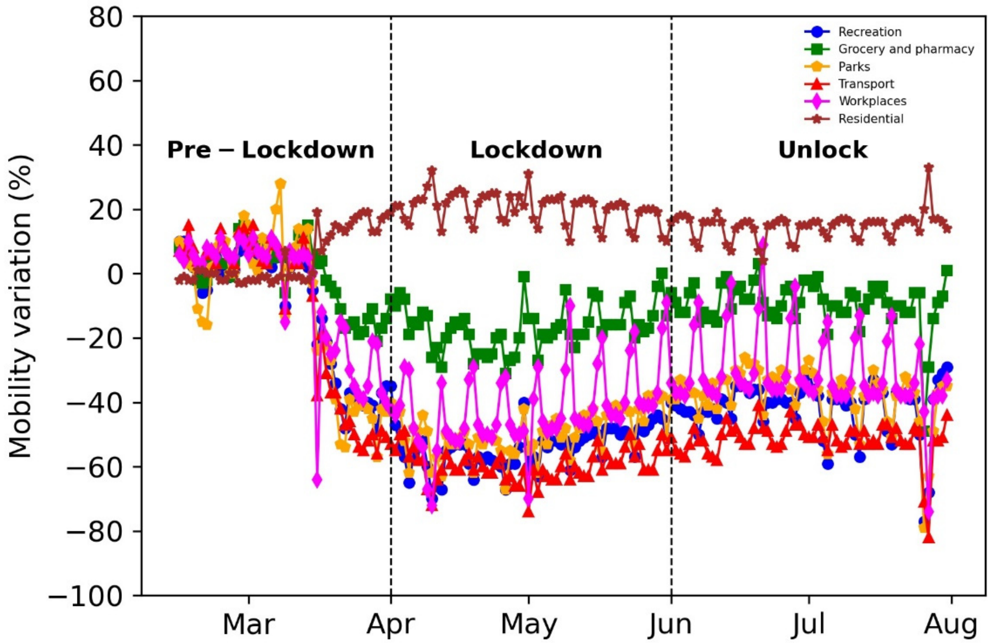

Figure 2. Mobility variation indicator compared to baseline (zero value) in Monterrey. The black dotted line marks the beginning of the lockdown on 1 April 2020 and the end on 31 May 2020.

According to Google Mobility, once the substantial restrictions were over on 1 June, mobility slowly returned to growth but did not reach the levels before the pandemic. Compared to the baseline, the percentage of mobility during the UL phase was −51.6%, −41.5%, −37.8%, −30.7%, and −9.4% considering public transport, recreation, parks, workplaces, and grocery and pharmacy, respectively. As reported during L, UL has registered an opposite trend in residential mobility, with an increase in 14.8%. Concerning the L phase, the difference between residential mobility shows a decrease in 5.4% due to the resumption of activities. During the UL phase and considering all categories, excluding residential, the mobility decreased by about −34.2%. Moreover, the mobility in UL compared to the L phase increased by 10.1%.

3.2. Air Pollutant Variation during COVID-19 Pandemic

Table 3 shows the descriptive statistics of the average air pollutant concentrations at all monitoring stations for the long-term (control interval, 2017–2019) and short-term (pandemic year, 2020) period. Temporal variation of all studied contaminants was observed in air quality data collected daily for seven months from January to July (Figure 3). During the entire study period in 2020, the range concentration of CO, NO_2, SO_2, O_3, PM_{10}, and $PM_{2.5}$ were 0.2 to 1.3 ppm (mean of 0.47), 0.6 to 22.6 ppb (mean of 7.05), 3.3 to 14.5 ppb (mean of 5.77), 6.5 to 66.7 ppb (mean of 31.93), 16.6 to 125.4 μg m^{-3} (mean of 46.96), and 4.5 to 51.7 μg m^{-3} (mean of 19.72), respectively. The average concentration of CO, NO_2, SO_2, O_3, PM_{10}, and $PM_{2.5}$ during the L phase from 1 April to 30 May 2020, was 0.42 ppm, 5.1, 4.9, 40.1 ppb, 39.6, and 18.7 μg m^{-3}, respectively. On the other hand, during the PL phase from 1 January to 31 March 2020, the average concentration of 0.58 ppm, 13.1, 7.1, 26.9 ppb, 56.5, and 22.7 μg m^{-3} were respectively recorded. Lastly, the average concentrations of CO, NO_2, SO_2, O_3, PM_{10}, and $PM_{2.5}$ during the UL phase from 1 June to 30 July 2020 were 0.36 ppm, 4.6, 4.6, 31.1 ppb, 40.2, and 16.4 μg m^{-3}, respectively.

Table 3. Average concentration of air pollutants during Pre-Lockdown (1 January to 31 March), Lockdown (1 April to 31 May), and Unlock (1 June to 31 July) phases in 2020 and 2017–2019 control period.

2020	**Pre-Lockdown**	**Lockdown**	**Unlock**	**[a] Diff (%)**	**[b] Diff (%)**
CO (ppm)	0.58	0.42	0.36	−27.6	−14.1
NO_2 (ppb)	13.1	5.1	4.6	−61.1	−9.4
SO_2 (ppb)	7.1	4.9	4.6	−31.1	−6.2
O_3 (ppb)	26.9	40.1	31.1	49.2	−22.5
PM_{10} (μg m^{-3})	56.5	39.6	40.2	−30.1	1.5
$PM_{2.5}$ (μg m^{-3})	22.7	18.7	16.4	−17.5	−12.6
2017–2019					
CO (ppm)	0.62	0.46	0.43	−24.8	−7.0
NO_2 (ppb)	13.3	6.0	6.7	−54.8	11.1
SO_2 (ppb)	9.5	8.5	6.9	−11.1	−17.9
O_3 (ppb)	25.0	34.9	30.4	39.4	−12.8
PM_{10} (μg m^{-3})	67.6	56.9	53.1	−15.8	−6.7
$PM_{2.5}$ (μg m^{-3})	25.6	25.2	17.3	−1.7	−31.3

[a] Percent of the difference between the Pre-Lockdown and Lockdown periods. [b] Percent of the difference between the Lockdown and Unlock period.

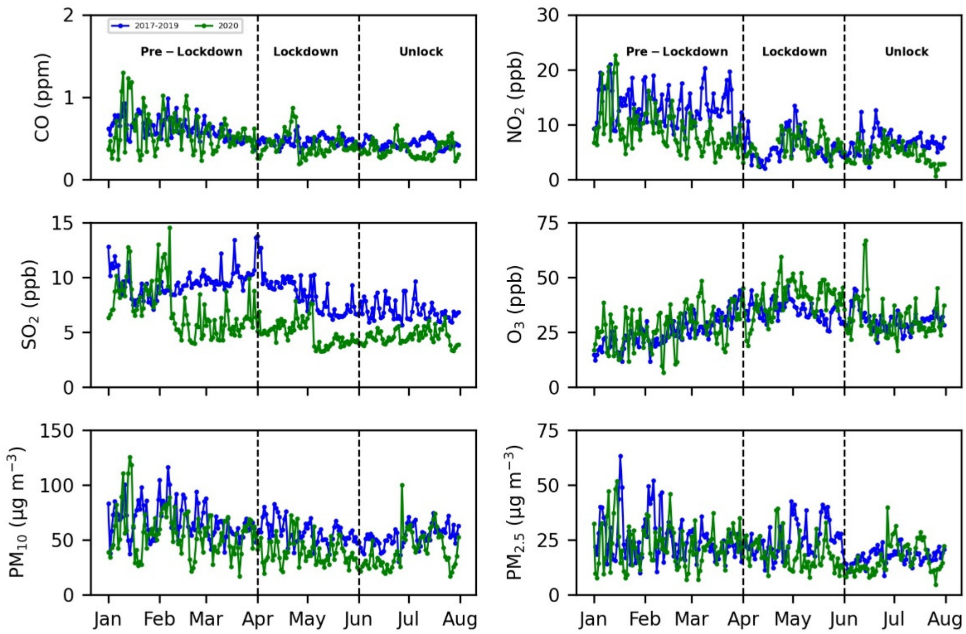

Figure 3. Daily average concentrations of CO, NO_2, SO_2, O_3, PM_{10}, and $PM_{2.5}$ between 1 January 2020 and 31 July 2020 (with lockdown starting on 1 April 2020 and ending 31 May 2020) and the previous three years (from 2017 to 2019) in Monterrey.

Comparing the difference between PL and L phases in the 2020 period, a significant decrease in the concentrations of contaminants is evident, except for O_3. NO_2 had the most significant decrease among the pollutants monitored at about −61%. An expected relative change is due to the reduction in vehicle circulation, the primary source of NO_2 emissions in urban areas [53]. NO_2 in MMA is also emitted to generate electricity, commercial activity, industry (manufacturing and mining activity), combustion of gas and oil, and aviation. CO is another contaminant gas emitted by anthropogenic sources such as incomplete combustion of motor vehicles and plant waste burning [54], which registered a reduction by −27.6%. SO_2 and PM_{10} show a decrease in −31.1% and −30.1%, respectively, mainly due to the deceleration of industrial processes and petroleum combustion [55,56]. SO_2, in addition to being emitted by oil refinery and vehicular traffic, is released by an industrial process, which had a ~30% decrease locally (−33% construction and −31% manufacturing). The restrictions affected economic activities and industrial processes and led to a decrease in $PM_{2.5}$ of −17.5%. Besides, possible local source appointment of $PM_{2.5}$ could be domestic and biomass burning emissions. However, diesel gasoline combustion from vehicles and energy production are the dominant sources of $PM_{2.5}$.

The PM_{10} variations in the atmosphere can also be affected by long-range transport from remote areas, principally in cities situated in arid and semiarid environments [57], instead, $PM_{2.5}$ is more likely to come from a local source [58]. O_3, a secondary pollutant, exhibits a completely different behavior than the other gases, increasing by 49.2%. The pollutant, such as NO_2 and NO_x compounds, joined with the presence of volatile organic carbon (VOC), emitted from chemical and power plants, industrial refineries, and traffic, react with sunlight to form tropospheric O_3 [59]. The isolation period and high temperature might have intensified the O_3 atmospheric concentration. Although O_3 increase has been reported in various parts of the world [60,61], its chemical complexity and formation process in the atmosphere under different conditions need to be investigated more in-depth. Moreover, comparing L with UL phases in 2020, a further decrease in gas concentration was recorded, except for PM_{10}. The reduction in CO, NO_2, SO_2, and $PM_{2.5}$ were −14.1%, −9.4%, −6.2%, and −12.6%, respectively. Although the strongest restrictions were over, the resumption of activities took a long time. In the UL phase, remote working was strongly recommended for businesses and public administration. Moreover, the schools and universities continued to carry out regular teaching activities through online connections. The concentration of O_3 shows a decrease compared to the L phase, expressed by a difference of −22.5% between phases. In this case, several factors can affect the variation of O_3 in the urban environment, such as the presence of a high concentration of nitric oxide (NO) and NO_x compounds that favor its partial depletion [62]. In this phase, PM_{10} was the only pollutant that recorded a slight increase in 1.5%, probably due to partially restarting some activities such as industrial, agricultural, and construction sites, a typical source in urban environments.

Pearson's correlation coefficient (r) was calculated to emphasize the relationships between the studied pollutant [63]. The results of the correlation matrix are shown in Figure 4 through an annotated heatmap. A significant positive correlation at $p < 0.05$ was found between several atmospheric gases. In the study period, from January to July 2020, analyzed gases significantly correlate with each other, indicating similar pollution sources and interactions. CO positively correlated with NO_2, SO_2, PM_{10}, and $PM_{2.5}$ (0.79, 0.53, 0.67, and 0.67, respectively). Besides, NO_2 was strongly correlated with SO_2, PM_{10}, and $PM_{2.5}$ (0.72, 0.73, and 0.61, respectively). SO_2 was strongly correlated with PM_{10} (0.62) and weakly correlated with $PM_{2.5}$ (0.43). A significative correlation (0.82) between PM_{10} and $PM_{2.5}$ are also observed. On the other hand, as seen in Figure 4, O_3 shows a negative significative correlation with CO, NO_2, SO_2, PM_{10}, and $PM_{2.5}$ (−0.33, −0.28, −0.26, −0.25, and −0.25, respectively). The negative correlation of O_3 may be due to the opposite concentration trend concerning other contaminants recorded during the various periods considered in this work.

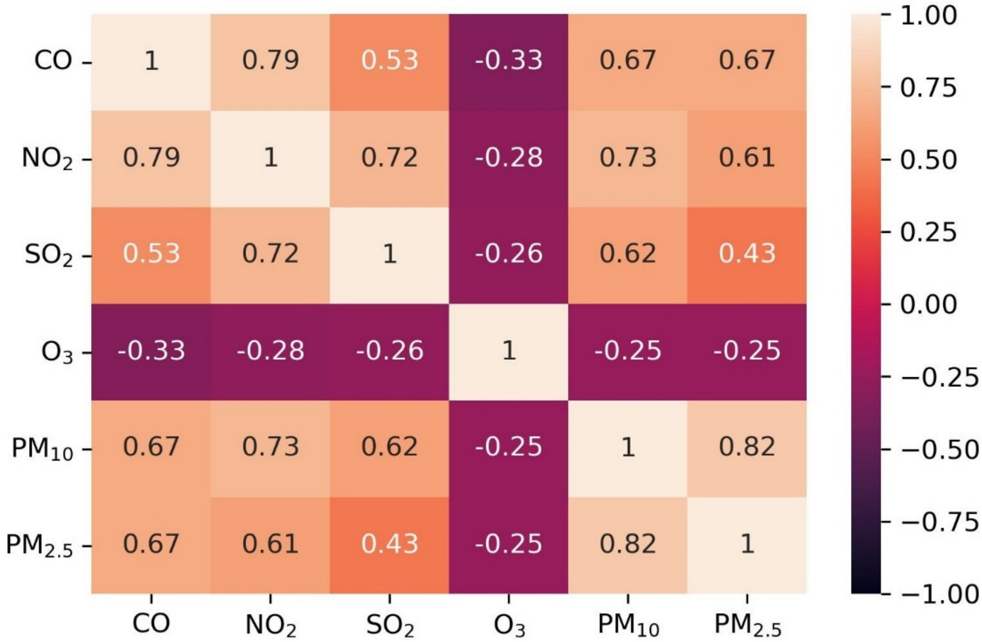

Figure 4. Annotated heatmap of a Pearson correlation matrix analysis between air pollutants in the study period during 2020.

3.3. Comparison with the Control Period

The control period, which starts in January 2017 and finishes in July 2019, was used as a background level to distinguish the anthropogenic signal in the urban environment during COVID-19 restrictions. Therefore, the difference between the measured period and background for a given time interval is considered as the changes in the anthropogenic contribution of the observed gas concentrations.

During the entire control period (Table 3), the range concentration of CO, NO_2, SO_2, O_3, PM_{10}, and $PM_{2.5}$ were 0.3 to 1 ppm (mean of 0.52), 2 to 21 ppb (mean of 9.27), 5.6 to 13.7 ppb (mean of 8.47), 11.6 to 46.1 ppb (mean of 29.4), 30 to 116.4 μg m^{-3} (mean of 60.3), and 8.6 to 63.2 μg m^{-3} (mean of 23.1), respectively. The average concentration of CO, NO_2, SO_2, O_3, PM_{10}, and $PM_{2.5}$ during the L phase from 1 April to 30 May 2017–2019 was 0.46 ppm, 6, 8.5, 34.9 ppb, 56.9, and 25.2 μg m^{-3}, respectively. On the other hand, during the PL phase from 1 January to 31 March 2017–2019, an average concentration of 0.62 ppm, 13.3, 9.5, 25 ppb, 67.6, and 25.6 μg m^{-3} were recorded, respectively. Lastly, the average concentrations of CO, NO_2, SO_2, O_3, PM_{10}, and $PM_{2.5}$ during the UL phase from 1 June to 30 July 2017–2019 were 0.43 ppm, 6.7, 6.9, 30.4 ppb, 53.1, and 17.3 μg m^{-3}, respectively. The comparison between the L phase in 2020 and the same period in 2017–2019 (Table 4) also shows a strong decrease for SO_2, followed by PM_{10}, $PM_{2.5}$, NO_2, and CO. Instead, O_3 is the only contaminant that registers an increase. Reductions are significant for PM_{10}, $PM_{2.5}$, and SO_2 with an average depletion of −30.5%, −25.6%, and −41.9%, respectively. Instead, a slight reduction was reported for CO and NO_2, with an average depletion of −9.8% and −14.9%, respectively. On the contrary, O_3 shows an increase in 15.0% compared to the same interval in the control period. In general, the recorded reductions are mainly due to the shut-off of industrial activities, sources of SO_2, NO_2, and PM_x emissions, and road traffic sources of NO_2, CO, and $PM_{2.5}$. Therefore, considering the air pollutants studied, excluding O_3, the total contamination reduction was 24.5%. The PL phase shows a reduction in atmospheric contaminant compared to the control period, especially evident for SO_2 (−25%) and followed by PM_{10} (−16.3%), $PM_{2.5}$ (−11.4%), CO (−6.2%), and NO_2 (−1.2%). The slight reduction in NO_2 may be due to the partial decrease in non-essential activities in March 2020, before L restrictions. Considering only the months of January and February 2020, the variations of concentrations are very similar, and no reduction has been recorded. Again, the O_3 shows an opposite trend compared to the other compounds, growing by

7.4%. The contaminants, excluding O_3, decreased by about 12% when comparing the PL phase between 2020 and the control period. Finally, the comparison between the 2020 and 2017–2019 background period during the UL phase shows an interesting trend of air pollutants. The increase in O_3 is due to the fact that its production depends on the concentration of its precursors, such as CO, NO_2, and VOCs. Observing that CO and NO_2 decreased their concentrations, VOCs had to be the main ozone precursor gases. In the absence of emissions, NO_2 is rapidly depleted, and the OH radical preferentially react with VOCs to form O_3. Sanitation measures during the pandemic period may have led to increased use of cleaning products, which contain reactive VOCs, alcohol, and chloride. In addition, VOC emissions by evaporation must be taken into account since March and April have been warmer in recent years. The same can be said of biogenic VOCs [60].

Table 4. Comparison of relative change (%) during 2020 Pre-Lockdown, Lockdown, and Unlock phases and the same time interval in the control period of 2017–2019.

	CO	**NO_2**	**SO_2**	**O_3**	**PM_{10}**	**$PM_{2.5}$**
Pre-Lockdown (1 January to 31 March)	−6.2	−1.2	−25.0	7.4	−16.3	−11.4
Lockdown (1 April to 31 May)	−9.8	−14.9	−41.9	15.0	−30.5	−25.6
Unlock (1 June to 31 July)	−16.6	−30.6	−33.6	2.2	−24.4	−5.4

As reported by PL and L phases, SO_2 presents the most significant reduction, followed by NO_2, PM_{10}, CO, and $PM_{2.5}$. The SO_2, PM_{10}, and $PM_{2.5}$ decrease by −30.6%, −24.4%, and −5.4%, respectively, even in smaller quantities than the restriction period, a sign of a slight recovery of activity (e.g., coal combustion, natural gas processing, and commercial activity, among others) which produce these types of emissions. On the other hand, the CO and NO_2 variation indicate a further reduction compared to the L phase, about −16.6% and −30.6%, respectively. The O_3 shows an increase in 2.2%, lower than the percentage registered in prior phases. Hence, considering total pollutants, except O_3, contamination decreased by about 22.1% compared to the same period of 2020 and the control interval period.

3.4. Comparison with Literature

The results observed in MMA are in line with the recently published literature. Reducing human and industrial activities during 2020 has improved air quality worldwide due to decreased pollution emissions [38,64–67]. In Tehran City, the most reduction was registered for NO_2 (1–33%) and CO (5–41%), followed by PM_{10} (1.4–30%) and SO_2 (5–28%). The most important result concerns the O_3, which had an increase in up to 103% [64]. In London, Vega et al. [24] describe various pollutants, such as NO_2 and $PM_{2.5}$, which achieve a decrease by 45%. Kurami and Toshniwal [68] described a significant decrease in concentration, between 19% and 60%, of PM_x, NO_2, and SO_2 in Delhi, India. In five highly polluting regions of India, significant decreases have been reported, especially for PM_{10} and $PM_{2.5}$, 31 and 43%, respectively [65]. Meanwhile, in the megacity of Sao Paulo, Brazil, the concentration of PM_x and NO_2 also decreased by approximately 45% and 58%, respectively [69]. Among the world capitals, Bogotá registered a significant $PM_{2.5}$ reduction in approximately 50% [70]. In some cases, O_3 has shown an opposite trend compared to other contaminated gases [48,71–73], increasing between 20 and 30%. This result shows the complexity of O_3 related to its formation, dispersion, and reaction with another air pollutant. Rodríguez-Urrego and Rodríguez-Urrego [70] reported an average reduction by 12% in contamination emissions by analyzing several cities (~50) around the world. Results from satellite [74] and ground-based data show an air quality improvement of 20–40% by selected pollutant ($PM_{2.5}$, PM_{10}, and NO_2) in European cities during the lockdown period [75,76].

A different evaluation is related to air quality studies in Mexico during the 2020 pandemic. Important gaps of data are present in the existing literature regarding the variations of air contaminants in Mexican megacities during the lockdown. To date, Mexico City was the only megacity covered by air quality studies in the period of several restrictions (i.e., lockdown due to the COVID-19 outbreak). Vega et al. [24] reported a significant decrease in several air pollutants during the lockdown period. CO registered the most significant decrease, of about −44.8% in both lockdown periods take into consideration, followed by NO_2 (−36.8%), $PM_{2.5}$ (−17.1%), and PM_{10} (−16.3%). As reported in our work, O_3 in Mexico City was the only contaminant that recorded an increase during the confinement period of about +6.5%. Compared to Mexico City, in MMA, the variation of pollutants registered a relatively minor decrease. On the contrary, O_3 had a larger increase in MMA than Mexico City, which may be due to various factors, especially local differences such as climate and source of pollutants.

3.5. Evaluation of Air Quality

As shown in the previous sections, air quality in the Monterrey area has improved considerably during the lockdown. Considering the normativity established by the Mexican government, reported in Table 2, the CO and SO_2 show relatively low concentrations and do not exceed the limits of the Mexican norm during 2020. Furthermore, the concentrations are lower than the WHO recommendations on an average value of 24 h. Especially for SO_2, this result is due to energy policies agreement by governments worldwide, reducing the content in fuels and consequently its emissions into the atmosphere [77]. NO_2 concentrations do not exceed the Mexican norm's limits but show values higher than the recommendations released by WHO. On the 24 h average, NO_2 exceeds the limits of 10 days only during the PL phase. In addition, the annual mean of NO_2 is 1.4 times higher than the limit value suggested by WHO. Following the norm provided by the Mexican government, O_3 exceeds the average hourly limit 46 times. On the other hand, considering the 8 h average, O_3 surpassed the limit 9 and 58 times in the entire period, according to the Mexican norms and WHO recommendations, respectively. The PM_{10} concentrations exceed the 24 h limit of the Mexican norms and WHO on several occasions, about 86 and 102, respectively. Moreover, the annual limit was 1.3 times higher according to the Mexican norm and 3.1 times higher than WHO recommendations. The variations of $PM_{2.5}$ follow the same trend as PM_{10}, exceeding the limit of 24 h in 26 days, according to the Mexican norm, and 136 days, conforming to WHO suggestion. Compared with the annual limit established by the Mexican norm and WHO, the concentration of $PM_{2.5}$ was 1.9 and 3.9 times higher, respectively.

The average AQI based on the concentrations of CO, NO_2, SO_2, O_3, PM_{10}, and $PM_{2.5}$ in MMA is shown in Table 5. Considering the average AQI values reported for the entire period (1 January to 31 July 2020), all pollutants, except $PM_{2.5}$, are in the range of 0–50, which returns a good air quality. Instead, $PM_{2.5}$ obtained an average value of 67, which means moderate air quality. The AQI results of CO, NO_2, SO_2, and O_3 in different pandemic phases (i.e., PL, L, and UL) showed good air quality with values less than 50. The PM_{10} also exhibits a moderate AQI with a value of 51 in the PL phase. On the other hand, good air quality was determined during L and UL phases. The evaluation of $PM_{2.5}$ concentrations returns a moderate AQI during all studied periods with values in the range of 51 and 100. The AQI analysis showed a significant improvement in the air quality of studied contaminants in the L and UL phases compared to PL. During the control period, the values of AQI were similar in the PL, whereas, in L, a drastic decrease was observed. Comparing the AQI average value between the 2020 and 2017–2019 periods during the L phase, the improvement was around 16.6%, 45.4%, 29.4%, and 17.7% for NO_2, SO_2, PM_{10}, and $PM_{2.5}$, respectively. CO did not show a difference between 2020 and the control period. Instead, the AQI values for O_3 record an increase in 19.3%. In previous studies, as reported in this work, a significant decrease in the AQI during restriction periods implemented to prevent the spread of COVID-19 was observed [38,69,78].

Table 5. Comparison of average AQI values distribution of several pollutants during Pre-Lockdown, Lockdown, and Unlock.

	CO	NO_2	SO_2	O_3	PM_{10}	$PM_{2.5}$
2020						
Pre-Lockdown	6	12	10	24	51	73
Lockdown	5	5	6	37	36	65
Unlock	3	4	6	29	37	60
2017–2019						
Pre-Lockdown	7	12	13	23	57	79
Lockdown	5	6	11	31	51	79
Unlock	5	6	9	28	49	62

AQI = Good: 0–50; Moderate: 51–100; Unhealthy for a sensitive group: 101–150.

3.6. Satellite Measurements

The satellite product of NO_2 tropospheric column density was considered to compare and validate ground-based monitoring stations in the MMA. The column density of NO_2 in the entire period (Figure 5), from January to July 2020, shows an average value of 1.43×10^{15} molecules cm^{-2} and ranges between 4.30×10^{14} and 3.49×10^{15} molecules cm^{-2}. Before the restrictive measures were implemented in the first analyzed period (from 1 January to 31 March), the average highest tropospheric column was obtained with the value of 2.02×10^{15} molecules cm^{-2}. The most important difference was found in the intermediate period (from 1 April to 31 May), in which severe cautionary measures were activated, estimating an average tropospheric column of 1.53×10^{15} molecules cm^{-2}. After the end of preventive measures, the last period (from 1 June to 31 July) presented a lower average column density of 1.43×10^{15} molecules cm^{-2}. A remarkable decrease in NO_2 tropospheric column density during the L and UL phases was found, probably due to traffic and industrial activity reduction. A reduction by around −24.2% was observed in the L compared to the PL phase, while a relatively low decrease in −6.5% was detected between L and UL phases. Comparing the satellite and ground-based measurements during L, the NO_2 level was estimated to be 2.5 times lower than the data reported by fixed stations; instead, it was 1.4 times lower than the value in the UL phase. Represa et al. [79] and Rendana [45] also reported a decrease in levels of NO_2 total column by remote sensing analysis in areas where quarantine for coronavirus was applied. Furthermore, the analyzed data revealed that: (i) comparing the value of NO_2 in the 2017–2019 period during the PL phase (1.98×10^{15} molecules cm^{-2}) and 2020, an increase in 2% was recorded; (ii) the average NO_2 tropospheric level in the control period during L phase (1.56×10^{15} molecules cm^{-2}) show a decrease in −1.9% compared to the same period in 2020; and (iii) a further decrease in −4.6% was recorded between the average NO_2 column density in control period (1.50×10^{15} molecules cm^{-2}) and 2020 during UL phase.

Satellite data retrievals of NO_2 showed substantial reduction mainly from the first days of L and the UL phase, evidencing the effects of the limitation in mobility (i.e., vehicular traffic) and social interactions in atmospheric pollutant elimination. Moreover, the decrease in industrial and commercial activity favored the improvement in air quality, also recorded with the satellite. A substantial difference in NO_2 reduction was found between satellite based-data retrieval and ground-measured data. The stations located on the surface return punctual values of the concentration of contaminants while the satellite analyzes an area with a given extension. In general, satellite data were used to validate data coming from ground stations, mainly due to satellite data having a high error component. The main errors concern the size of the pixel, the distance of the satellite from the earth's surface, the type of orbit, and the presence of clouds.

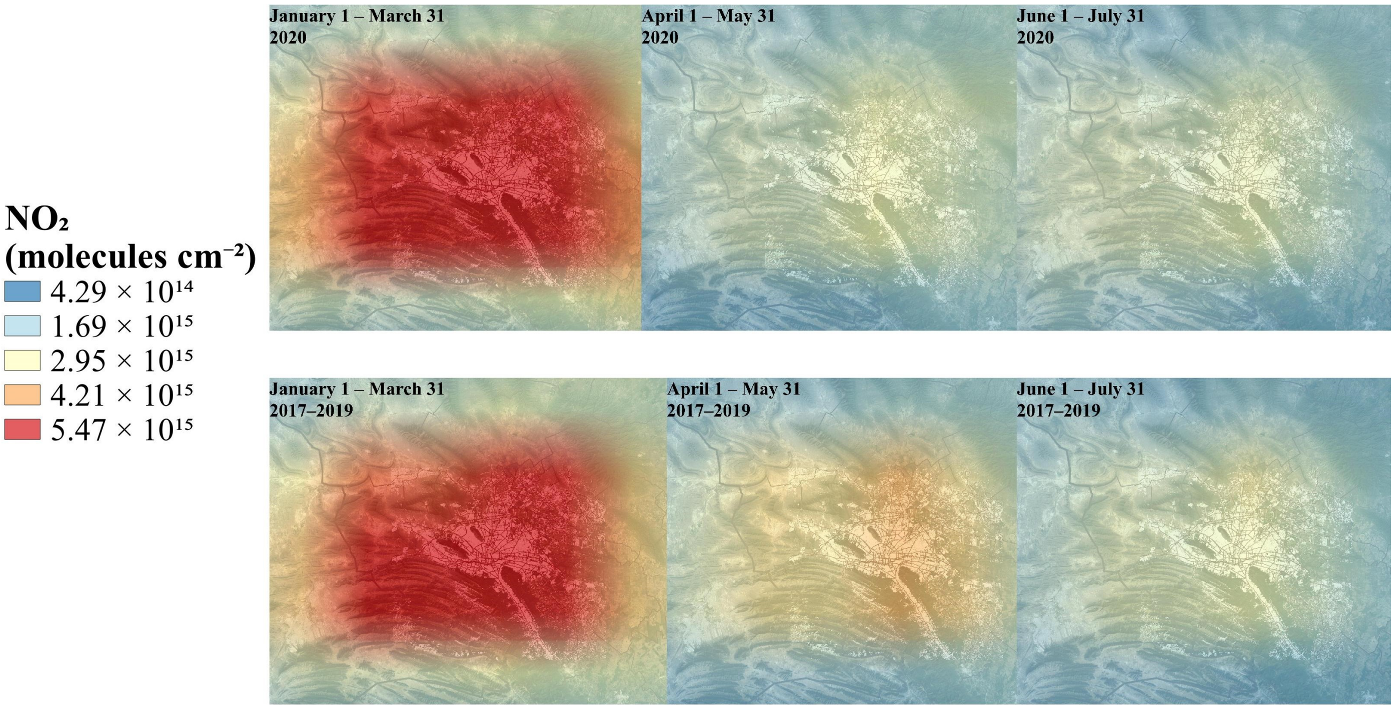

Figure 5. Average NO_2 tropospheric levels measured by OMI/AURA satellite during Monterrey's pre-lockdown, lockdown, and unlock phases. A comparison with the control period (2017–2019) is also reported.

4. Limitations of the Study

This study has the following limitations:

- Many studies have reported the connection between air contamination and the spread of COVID-19 cases [80,81]. Therefore, we investigated the variation of pollutants in the atmosphere of MMA during three periods (PL, L, and UL). However, it was impossible to implement the study by relating the incidence of COVID-19 cases in the population. Nevertheless, Zhu et al. [82] reported a significative correlation between confirmed cases and CO, NO_2, O_3, and aerosols.
- Atmospheric contamination and its dispersion depend on local meteorological conditions (temperature, pressure, intensity of radiation, wind speed, and direction). Therefore, its crucial to correlate air pollutants with meteorological data, which play a significant role in the chemical reaction in the atmosphere and could favor the increase in contamination. Furthermore, seasonal variations of contaminations and climate conditions during the COVID-19 outbreak must be analyzed in more detail.
- Comparing ground-based measurements and satellite data is an essential part of studies on atmospheric contamination. In this work, as reported by many authors [48,68,83], only NO_2 was used for the validation, being considered the main compound for determining the degree of contamination in urban environments. However, satellite validation with other compounds, such as SO_2 and PM, must be implemented to improve air quality monitoring and retrieval of pollutant concentration.

5. Conclusions and Recommendations

This work investigated the variation of atmospheric pollutants and urban air quality improvement due to recent COVID-19 pandemic measures was investigated in Monterrey city. The substantial mobility reduction, around −44%, and industrial activity shutdown allowed us to evaluate the atmospheric baseline of specific pollutants directly associated with anthropogenic emissions. Time series of CO, NO_2, SO_2, PM_{10}, and $PM_{2.5}$ during the 2020 quarantine phase showed a drastic reduction in their concentrations in the atmosphere concerning the 2017–2019 control period. On the contrary, O_3 registered an opposite trend compared to other contaminants, increasing during the lockdown. The concentration of air pollutants increased during the unlock phase when severe preventive measures were removed. However, the levels of contaminant gases remain lower than in the same period in 2017–2019. The AQI recorded a significant improvement, especially for NO_2, PM_{10}, and $PM_{2.5}$, during the lockdown and unlocked phases in 2020 and compared to the 2017–2019 control interval in the same period. The atmospheric levels of NO_2 obtained from the ground-based measurement were also validated with tropospheric OMI/AURA satellite data. Tropospheric NO_2 showed the same descending trend as the fixed stations during the lockdown phase, demonstrating the compatibility between ground-based and satellite measurements for air quality monitoring.

The lockdown period should be used as a baseline for air quality mitigation strategies. The period of restrictions has taught the whole world how reducing atmospheric contamination is possible by applying effective strategies. Future strategies must take into account a balance between economic activities and green public policies in favor of the environment. Local government should promote technological infrastructure, the creation of smart cities, work from home (e.g., online classes and virtual conferences), and the public diffusion of information related to environmental sustainability and public health. The use of renewable sources, such as solar and wind power, would be a first step towards relatively reducing anthropogenic emissions into the atmosphere. The next step could be to promote cyclist infrastructure and social programs for a non-motorized mode of transportation. This is considering that in the MMA, the main cause of contamination is vehicular traffic, approximately 45%. This scenario was a unique opportunity to determine the air pollutant emissions in urban areas and implement green social initiatives and mobility policies to reduce air pollution levels.

Author Contributions: Conceptualization: B.S., O.M.-B. and D.M.-F.; Data curation, T.E.A.-P. and B.G.-G.; Formal analysis, B.S. and T.E.A.-P.; Investigation, B.S. and R.G.-M.; Methodology, B.S. and T.E.A.-P.; Resources, O.M.-B.; Software, T.E.A.-P. and A.R.-M.; Supervision, O.M.-B. and D.M.-F.; Validation, B.S. and R.G.-M.; Visualization, B.S., A.R.-M., D.V.-F., C.I. and B.G.-G.; Writing—original draft, B.S.; Writing—review & editing, D.V.-F. and C.I. All authors have read and agreed to the published version of the manuscript.

Funding: This research received no funding.

Institutional Review Board Statement: This study did not require ethical approval.

Informed Consent Statement: Not applicable.

Data Availability Statement: The data presented in this study are available on request from the corresponding author.

Acknowledgments: The authors gratefully acknowledge M.C. Jair Rafael Carrillo Avila and the Sistema Integral de Monitoreo Ambiental (SIMA) for providing data for this study.

Conflicts of Interest: The authors declare no conflict of interest.

References

1. WHO. World Health Organization. Ambient Air Pollution: A global Assessment of Exposure and Burden of Disease. 2016. Available online: https://apps.who.int/iris/bitstream/handle/10665/250141/9789241511353-eng.pdf?sequence=1&isAllowed=y (accessed on 28 October 2022).
2. Burnett, R.; Chen, H.; Szyszkowicz, M.; Fann, N.; Hubbell, B.; Pope Iii, C.A.; Apte, J.S.; Brauer, M.; Cohen, A.; Weichenthal, S.; et al. Global estimates of mortality associated with long-term exposure to outdoor fine particulate matter. *Proc. Natl. Acad. Sci. USA* **2018**, *115*, 9592–9597. [CrossRef]
3. Nansai, K.; Tohno, S.; Chatani, S.; Kanemoto, K.; Kagawa, S.; Kondo, Y.; Takayanagi, W.; Lenzen, M. Consumption in the G20 nations causes particulate air pollution resulting in two million premature deaths annually. *Nat. Commun.* **2021**, *12*, 6286. [CrossRef]
4. Liang, L.; Gong, P. Urban and air pollution: A multi-city study of long-term effects of urban landscape patterns on air quality trends. *Sci. Rep.* **2020**, *10*, 18618. [CrossRef]

5. Kim, K.-H.; Kabir, E.; Kabir, S. A review on the human health impact of airborne particulate matter. *Environ. Int.* **2015**, *74*, 136–143. [CrossRef]
6. Ortega-Rosas, C.I.; Meza-Figueroa, D.; Vidal-Solano, J.R.; González-Grijalva, B.; Schiavo, B. Association of airborne particulate matter with pollen, fungal spores, and allergic symptoms in an arid urbanized area. *Environ. Geochem. Health* **2021**, *43*, 1761–1782. [CrossRef]
7. Li, T.; Hu, R.; Chen, Z.; Li, Q.; Huang, S.; Zhu, Z.; Zhou, L.-F. Fine particulate matter ($PM_{2.5}$): The culprit for chronic lung diseases in China. *Chronic Dis. Transl. Med.* **2018**, *4*, 176–186. [CrossRef]
8. Mamkhezri, J.; Bohara, A.K.; Camargo, I. Air pollution and daily mortality in the Mexico City Metropolitan Area. *Atmósfera* **2020**, *33*, 249–267. [CrossRef]
9. Romero-Lankao, P.; Qin, H.; Borbor-Cordova, M. Exploration of health risks related to air pollution and temperature in three Latin American cities. *Soc. Sci. Med.* **2013**, *83*, 110–118. [CrossRef]
10. Molina, L.T.; Molina, M.J. Improving Air Quality in Megacities: Mexico City Case Study. *Ann. N. Y. Acad. Sci.* **2004**, *1023*, 142–158. [CrossRef]
11. Baca-López, K.; Fresno, C.; Espinal-Enríquez, J.; Martínez-García, M.; Camacho-López, M.A.; Flores-Merino, M.V.; Hernández-Lemus, E. Spatio-Temporal Representativeness of Air Quality Monitoring Stations in Mexico City: Implications for Public Health. *Public Health Front.* **2021**, *8*, 536174. [CrossRef]
12. Morton-Bermea, O.; Hernández-Álvarez, E.; Almorín-Ávila, M.A.; Ordoñez-Godínez, S.; Bermendi-Orosco, L.; Retama, A. Historical trends of metals concentration in PM_{10} collected in the Mexico City metropolitan area between 2004–2014. *Environ. Geochem. Health* **2020**, *43*, 2781–2798. [CrossRef] [PubMed]
13. Fernández-Bremauntz, A. Air Quality Management in Mexico. *J. Toxicol. Environ. Health Part A* **2008**, *71*, 56–62. [CrossRef] [PubMed]
14. Molina, L.T.; Velasco, E.; Retama, A.; Zavala, M. Experience from Integrated Air Quality Management in the Mexico City Metropolitan Area and Singapore. *Atmosphere* **2019**, *10*, 512. [CrossRef]
15. Lu, H.; Stratton, C.W.; Tang, Y.-W. Outbreak of pneumonia of unknown etiology in Wuhan, China: The mystery and the miracle. *J. Med. Virol.* **2020**, *92*, 401–402. [CrossRef] [PubMed]
16. Cucinotta, D.; Vanelli, M. WHO Declares COVID-19 a Pandemic. *Acta Biomed.* **2020**, *91*, 157–160. [CrossRef]
17. Bonaccorsi, G.; Pierri, F.; Cinelli, M.; Flori, A.; Galeazzi, A.; Porcelli, F.; Schmidt, A.L.; Valensise, C.M.; Scala, A.; Quattrociocchi, W.; et al. Economic and social consequences of human mobility restrictions under COVID-19. *Proc. Natl. Acad. Sci. USA* **2020**, *117*, 15530–15535. [CrossRef]
18. Nicola, M.; Alsafi, Z.; Sohrabi, C.; Kerwan, A.; Al-Jabir, A.; Iosifidis, C.; Agha, M.; Agha, R. The socio-economic implications of the coronavirus pandemic (COVID-19): A review. *Int. J. Surg.* **2020**, *78*, 185–193. [CrossRef]
19. WHO. World Health Organization, Coronavirus Disease (COVID-2019) Situation Reports–Situation Report—Edition 100. 2022. Available online: https://www.who.int/publications/m/item/weekly-epidemiological-update-on-covid-19 (accessed on 13 July 2022).
20. Bautista-González, E.; Werner-Sunderland, J.; Mendiola, P.P.D.; Jeronimo Esquinca-Enríquez-de-la, C.; Bautista-Reyes, D.; Maciel-Gutiérrez, M.F.; Murguía-Arechiga, I.; Vindrola-Padros, C.; Urbina-Fuentes, M. Health-care guidelines and polities during the COVID-19 pandemic in Mexico: A case of health-inequalities. *Health Policy Open* **2021**, *2*, 100025. [CrossRef]
21. Fernández-Rojas, M.A.; Esparza, M.A.L.R.; Campos-Romero, A.; Calva-Espinosa, D.Y.; Moreno-Camacho, J.L.; Langle-Martínez, A.P.; García-Gil, A.; Solís-González, C.J.; Canizalez-Román, A.; León-Sicairos, N.; et al. Epidemiology of COVID-19 in Mexico: Symptomatic profiles and presymptomatic people. *Int. J. Infect. Dis.* **2021**, *104*, 572–579. [CrossRef]
22. MRC. Mexico's Response to COVID-19: A Case Study. Institute for Global Health Sciences. 2021. Available online: https://globalhealthsciences.ucsf.edu/sites/globalhealthsciences.ucsf.edu/files/mexico-covid-19-case-study-english.pdf (accessed on 28 October 2022).
23. Fan, H.; Wang, Y.; Zhao, C.; Yang, Y.; Yang, X.; Sun, Y.; Jiang, S. The Role of Primary Emission and Transboundary Transport in the Air Quality Changes During and After the COVID-19 Lockdown in China. *Geophys. Res. Lett.* **2021**, *48*, e2020GL091065. [CrossRef]
24. Vega, E.; Namdeo, A.; Bramwell, L.; Miquelajauregui, Y.; Resendiz-Martinez, C.G.; Jaimes-Palomara, M.; Luna-Falfan, F.; Terrazas-Ahumada, A.; Maji, K.J.; Entwistle, J.; et al. Changes in air quality in Mexico City, London and Delhi in response to various stages and levels of lockdowns and easing of restrictions during COVID-19 pandemic. *Environ. Pollut.* **2021**, *285*, 117664. [CrossRef] [PubMed]
25. Kutralam-Muniasamy, G.; Pérez-Guevara, F.; Roy, P.D.; Elizalde-Martínez, I.; Shruti, V.C. Impacts of the COVID-19 lockdown on air quality and its association with human mortality trends in megalopolis Mexico City. *Air Qual. Atmos. Health* **2021**, *14*, 553–562. [CrossRef] [PubMed]
26. INEGI. Instituto Nacional de Estadística y Geografía. Censo de Población y Vivienda. 2021. Available online: https://www.inegi.org.mx/contenidos/productos/prod_serv/contenidos/espanol/bvinegi/productos/nueva_estruc/702825198701.pdf (accessed on 15 October 2022).
27. Sisto, N.P.; Ramírez, A.I.; Aguilar-Barajas, I.; Magaña-Rueda, V. Climate threats, water supply vulnerability and the risk of a water crisis in the Monterrey Metropolitan Area (Northeastern Mexico). *Phys. Chem. Earth Parts A/B/C* **2016**, *91*, 2–9. [CrossRef]

28. *NOM-21. NOM-021-SSA1-1993*; Environmental Health. Criteria to Assess Air Quality of Ambient Air Regarding to Carbon Monoxide (CO). DOF: Mexico City, Mexico, 1993.
29. *NOM-20. NOM-020-SSA1-2014*; Environmental Health. Criteria to Assess Air Quality of Ambient Air Regarding to Ozone (O_3). DOF: Mexico City, Mexico, 2014.
30. WHO. World Health Organization Air Quality Guidelines Global Update 2005: Particulate Matter, Ozone, Nitrogen Dioxide and Sulfur Dioxide. WHO Regional Office for Europe, Copenhagen. 2006. Available online: https://apps.who.int/iris/handle/10665/107823 (accessed on 21 September 2022).
31. *NOM-21. NOM-021-SSA1-2021*; Environmental Health. Criteria to Assess Air Quality of Ambient Air Regarding to Carbon Monoxide (CO). DOF: Mexico City, Mexico, 2021. Available online: http://www.aire.cdmx.gob.mx/descargas/monitoreo/normatividad/NOM-021-SSA1-2021.pdf (accessed on 21 September 2022).
32. *NOM-23. NOM-023-SSA1-2021*; Environmental Health. Criteria to Assess Air Quality of Ambient Air Regarding to Nitrogen Dioxide (NO_2). DOF: Mexico City, Mexico, 2021. Available online: http://www.aire.cdmx.gob.mx/descargas/monitoreo/normatividad/NOM-023-SSA1-2021.pdf (accessed on 21 September 2022).
33. *NOM-22. NOM-022-SSA1-2019*; Environmental Health. Criteria to Assess Air Quality of Ambient Air Regarding to Sulfur Dioxide (SO_2). DOF: Mexico City, Mexico, 2019. Available online: http://www.aire.cdmx.gob.mx/descargas/monitoreo/normatividad/NOM-022-SSA1-2019.pdf (accessed on 21 September 2022).
34. *NOM-20. NOM-020-SSA1-2021*; Environmental Health. Criteria to Assess Air Quality of Ambient Air Regarding to Ozone (O_3). DOF: Mexico City, Mexico, 2021. Available online: http://www.aire.cdmx.gob.mx/descargas/monitoreo/normatividad/NOM-020-SSA1-2021.pdf (accessed on 21 September 2022).
35. *NOM-25. NOM-025-SSA1-2014*; Environmental Health. Criteria to Assess Air Quality of Ambient Air Regarding to Particles Minor than 10 Microns (PM_{10}) and Minor to 2.5 Microns ($PM_{2.5}$). DOF: Mexico City, Mexico, 2021. Available online: http://www.aire.cdmx.gob.mx/descargas/monitoreo/normatividad/NOM-025-SSA1-2021.pdf (accessed on 21 September 2022).
36. WHO. World Health Organization Air Quality Guidelines for Particulate Matter, Ozone, Nitrogen Dioxide and Sulfur Dioxide: Global Update. 2018. Available online: https://www.who.int/news-room/fact-sheets/detail/ambient-(outdoor)-air-quality-and-health (accessed on 30 September 2022).
37. WHO. World Health Organization, Ambient (Outdoor) Air Pollution Guidelines. 2021. Available online: https://apps.who.int/iris/bitstream/handle/10665/345329/9789240034228-eng.pdf (accessed on 30 September 2022).
38. Seo, J.H.; Kim, J.S.; Yang, J.; Yun, H.; Roh, M.; Kim, J.W.; Yu, S.; Jeong, N.N.; Jeon, H.W.; Choi, J.S.; et al. Changes in Air Quality during the COVID-19 Pandemic and Associated Health Benefits in Korea. *Appl. Sci.* **2020**, *10*, 8720. [CrossRef]
39. Mirabelli, M.C.; Ebelt, S.; Damon, S.A. Air Quality Index and air quality awareness among adults in the United States. *Environ. Res.* **2020**, *183*, 109185. [CrossRef]
40. Keshtkar, M.; Heidari, H.; Moazzeni, N.; Azadi, H. Analysis of changes in air pollution quality and impact of COVID-19 on environmental health in Iran: Application of interpolation models and spatial autocorrelation. *Environ. Sci. Pollut. Res.* **2022**, *29*, 38505–38526. [CrossRef]
41. Schiavo, B.; Stremme, W.; Grutter, M.; Campion, R.; Guarin, C.A.; Rivera, C.; Inguaggiato, S. Characterization of a UV camera system for SO_2 measurements from Popocatépetl Volcano. *J. Volcanol. Geotherm. Res.* **2019**, *370*, 82–94. [CrossRef]
42. Google. COVID-19 Community Mobility Reports. 2020. Available online: https://www.google.com/covid19/mobility/ (accessed on 15 October 2022).
43. Krotkov, N.A.; McLinden, C.A.; Li, C.; Lamsal, L.N.; Celarier, E.A.; Marchenko, S.V.; Swartz, W.H.; Bucsela, E.J.; Joiner, J.; Duncan, B.N.; et al. Aura OMI observations of regional SO2 and NO2 pollution changes from 2005 to 2015. *Atmos. Chem. Phys.* **2016**, *16*, 4605–4629. [CrossRef]
44. Naeem, W.; Kim, J.; Lee, Y.G. Spatiotemporal Variations in the Air Pollutant NO2 in Some Regions of Pakistan, India, China, and Korea, before and after COVID-19, Based on Ozone Monitoring Instrument Data. *Atmosphere* **2022**, *13*, 986. [CrossRef]
45. Rendana, M. Air Pollutant Levels during the Large-scale Social Restriction Period and its Association with Case Fatality Rate of COVID-19. *Aerosol Air Qual. Res.* **2021**, *7*, 200630. [CrossRef]
46. van Rossum, G.; de Boer, J. Interactively Testing Remote Servers Using the Python Programming Language. *CWI Q.* **1991**, *4*, 283–303. Available online: https://ir.cwi.nl/pub/18204 (accessed on 19 November 2022).
47. Deville, P.; Song, C.; Eagle, N.; Blondel, V.D.; Barabási, A.-L.; Wang, D. Scaling identity connects human mobility and social interactions. Applied Physical Sciences. *Proc. Natl. Acad. Sci. USA* **2016**, *113*, 7047–7052. [CrossRef] [PubMed]
48. Teixidó, O.; Tobías, A.; Massagué, J.; Mohamed, R.; Ekaani, R.; Hamed, H.I.; Perry, R.; Querol, X.; Hosani, S.A. The influence of COVID-19 preventive measures on the air quality in Abu Dhabi (United Arab Emirates). *Air Qual. Atmos. Health* **2021**, *14*, 1071–1079. [CrossRef] [PubMed]
49. Hakim, A.J.; Victory, K.R.; Chevinsky, J.R.; Hast, M.A.; Weikum, D.; Kazazian, L.; Mirza, S.; Bhatkoti, R.; Schmitz, M.M.; Lynch, M.; et al. Mitigation polities, community mobility, and COVID-19 case counts in Australia, Japan, Hong Kong, and Singapore. *Public Health* **2021**, *194*, 238–244. [CrossRef] [PubMed]
50. Saha, J.; Barman, B.; Chouhan, P. Lockdown for COVID-19 and its impact on community mobility in India: An analysis of the COVID-19 Community Mobility Reports, 2020. Child. *Youth Serv. Rev.* **2020**, *116*, 105160. [CrossRef] [PubMed]
51. Nouvellet, P.; Bhatia, S.; Cori, A.; Ainslie, K.E.; Baguelin, M.; Bhatt, S.; Boonyasiri, A.; Brazeau, N.F.; Cattarino, L.; Cooper, L.V.; et al. Reduction in mobility and COVID-19 transmission. *Nat. Commun.* **2021**, *12*, 1090. [CrossRef] [PubMed]

52. Mitra, D.; Chu, Y.; Cetin, K. COVID-19 impacts on residential occupancy schedules and activities in U.S. Homes in 2020 using ATUS. *Appl. Energy* **2022**, *324*, 119765. [CrossRef]
53. Lamsal, L.N.; Martin, R.V.; Parrish, D.D.; Krotkov, N.A. Scaling Relationship for NO_2 Pollution and Urban Population Size: A Satellite Perspective. *Environ. Sci. Technol.* **2013**, *47*, 7855–7861. [CrossRef]
54. Penache, M.; Zoran, M. Seasonal trends of surface carbon monoxide concentrations in relation with air quality. *AIP Conf. Proc.* **2019**, *2075*, 130007. [CrossRef]
55. Smith, S.J.; van Aardenne, J.; Klimont, Z.; Andres, R.J.; Volke, A.; Delgado Arias, S. Anthropogenic sulfur dioxide emissions: 1850–2005. *Atmos. Chem. Phys.* **2011**, *11*, 1101–1116. [CrossRef]
56. Reizer, M.; Juda-Rezler, K. Explaining the high PM10 concentrations observed in Polish urban areas. *Air Qual. Atmos. Health* **2016**, *9*, 517–531. [CrossRef] [PubMed]
57. Guan, Q.; Yang, Y.; Luo, H.; Zhao, R.; Pan, N.; Lin, J.; Yang, L. Transport pathways of PM_{10} during the spring in northwest China and its characteristics of potential dust sources. *J. Clean. Prod.* **2019**, *237*, 117746. [CrossRef]
58. Tessum, M.W.; Anenberg, S.C.; Chafe, Z.A.; Henze, D.K.; Kleiman, G.; Kheirbek, I.; Marshall, J.; Tessum, C.W. Sources of ambient $PM_{2.5}$ exposure in 96 global cities. *Atmos. Environ.* **2022**, *286*, 119234. [CrossRef] [PubMed]
59. Paoletti, E.; de Marco, A.; Beddows, D.C.S.; Harrison, R.M.; Manning, W.J. Ozone levels in Europe and USA cities are increasing more than at rural sites, while peak values are decreasing. *Environ. Pollut.* **2014**, *192*, 295–299. [CrossRef]
60. Peralta, O.; Ortínez-Alvarez, A.; Torres-Jaron, R.; Suárez-Lastra, M.; Castro, T.; Ruíz-Suárez, L.G. Ozone over Mexico City during the COVID-19 pandemic. *Sci. Total Environ.* **2021**, *761*, 143183. [CrossRef]
61. Rathod, A.; Sahu, S.K.; Singh, S.; Beig, G. Anomalous behavior of ozone under COVID-19 and explicit diagnosis of O_3-NO_x-VOCs mechanism. *Heliyon* **2021**, *7*, e06142. [CrossRef] [PubMed]
62. Sicard, P.; Paoletti, E.; Agathokleous, E.; Araminienė, V.; Proietti, C.; Coulibaly, F.; De Marco, A. Ozone weekend effect in cities: Deep insights for urban air pollution control. *Environ. Res.* **2020**, *191*, 110193. [CrossRef] [PubMed]
63. Pant, G.; Garlapati, D.; Gaur, A.; Hossain, K.; Singh, S.V.; Gupta, A.K. Air quality assessment among populous sites of major metropolitan cities in India during COVID-19 pandemic confinement. *Environ. Sci. Pollut. Res.* **2020**, *27*, 44629–44636. [CrossRef]
64. Broomandi, P.; Karaca, F.; Nikfal, A.; Jahanbakhshi, A.; Tamjidi, M.; Kim, J.R. Impact of COVID-19 event on the air quality in Iran. *Aerosol Air Qual. Res.* **2020**, *20*, 1793–1804. [CrossRef]
65. Sharma, S.; Zhang, M.; Anshika Gao, J.; Zhang, H.; Kota, S.H. Effect of restricted emissions during COVID-19 on air quality in India. *Sci. Total Environ.* **2020**, *728*, 138878. [CrossRef]
66. Venter, Z.S.; Aunan, K.; Chowdhury, S.; Lelieveld, J. COVID-19 lockdowns cause global air pollution declines. *Proc. Natl. Acad. Sci. USA* **2020**, *117*, 18984–18990. [CrossRef] [PubMed]
67. Wang, P.; Chen, K.; Zhu, S.; Wang, P.; Zhang, H. Severe air pollution events not avoided by reduced anthropogenic activities during COVID-19 outbreak. *Resour. Conserv. Recycl.* **2020**, *158*, 104814. [CrossRef] [PubMed]
68. Kumari, P.; Toshniwal, D. Impact of lockdown measures during COVID-19 on air quality—A case study of India. *Int. J. Environ. Health Res.* **2020**, *32*, 503–510. [CrossRef] [PubMed]
69. Debone, D.; da Costa, M.V.; Miraglia, S.G.E.K. 90 Days of COVID-19 Social Distancing and Its Impacts on Air Quality and Health in Sao Paulo, Brazil. *Sustainability* **2020**, *12*, 7440. [CrossRef]
70. Rodríguez-Urrego, D.; Rodríguez-Urrego, L. Air quality during the COVID-19: $PM_{2.5}$ analysis in the 50 most polluted capital cities in the world. *Environ. Pollut.* **2020**, *266*, 115042. [CrossRef]
71. Becerra-Rondón, A.; Ducati, J.; Haag, R. Partial COVID-19 lockdown effect in atmospheric pollutants and indirect impact in UV radiation in Rio Grande do Sul, Brazil. *Atmósfera* **2022**, *36*, 143–154. [CrossRef]
72. Campbell, P.C.; Tong, D.; Tang, Y.; Baker, B.; Pius, L.; Saylor, R.; Stein, A.; Ma, S.; Lamsal, L.; Qu, Z. Impacts of the COVID-19 economic slowdown on ozone pollution in the U.S. *Atmos. Environ.* **2021**, *264*, 118713. [CrossRef]
73. Zhang, K.; Liu, Z.; Zhang, X.; Li, Q.; Jensen, A.; Tan, W.; Huang, L.; Wang, Y.; de Gouw, J.; Li, L. Insights into the significant increase in ozone during COVID-19 in a typical urban city of China. *Atmos. Chem. Phys.* **2022**, *22*, 4853–4866. [CrossRef]
74. Khan, I.; Shah, D.; Shah, S.S. COVID-19 pandemic and its positive impacts on environment: An update review. *Int. J. Environ. Sci. Technol.* **2021**, *18*, 521–530. [CrossRef]
75. Polednik, B. Air quality changes in a Central European city during COVID-19 lockdown. Sustain. *Cities Soc.* **2021**, *73*, 103096. [CrossRef]
76. Skirienė, A.F.; Stasiškienė. COVID-19 and Air Pollution: Measuring Pandemic Impact to Air Quality in Five European Countries. *Atmosphere* **2021**, *12*, 290. [CrossRef]
77. Nurrohim, A.; Sakugawa, H. Fuel-based inventory of NO_x and SO_2 emissions from motor vehicles in the Hiroshima Prefecture, Japan. *Appl. Energy* **2005**, *80*, 291–305. [CrossRef]
78. Xu, K.; Cui, K.; Young, L.-H.; Wang, Y.-F.; Hsieh, Y.-K.; Wan, S.; Zhang, J. Air quality index, indicatory air pollutants and impact of COVID-19 event on the air quality near central China. *Aerosol Air Qual. Res.* **2020**, *20*, 1204–1221. [CrossRef]
79. Represa, N.S.; Della Ceca, L.S.; Abril, G.; García Ferreyra, M.F.; Scavuzzo, C.M. Atmospheric Pollutants Assessment during the COVID-19 Lockdown Using Remote Sensing and Ground-based Measurements in Buenos Aires, Argentina. *Aerosol Air Qual. Res.* **2021**, *21*, 200486. [CrossRef]
80. Carballo, I.H.; Bakola, M.; Stuckler, D. The impact of air pollution on COVID-19 incidence, severity, and mortality: A systematic review of studies in Europe and North America. *Environ. Res.* **2022**, *215*, 114155. [CrossRef]

81. Travaglio, M.; Yu, Y.; Popovic, R.; Selley, L.; Leal, N.S.; Martins, L.M. Links between air pollution and COVID-19 in England. *Environ. Pollut.* **2021**, *268*, 115859. [CrossRef]
82. Zhu, Y.; Xie, J.; Huang, F.; Cao, L. Association between short-term exposure to air pollution and COVID-19 infection: Evidence from China. *Sci. Total Environ.* **2020**, *727*, 138704. [CrossRef]
83. Toro, R.; Catalán, F.; Urdanivia, F.R.; Rojas, J.P.; Manzano, C.A.; Seguel, R.; Gallardo, L.; Osses, M.; Pantoja, N.; Leiva-Guzman, M.A. Air pollution and COVID-19 lockdown in a large South American city: Santiago Metropolitan Area, Chile. *Urban Clim.* **2021**, *36*, 100803. [CrossRef]